

Picosecond laser fabrication of nanostructures on ITO film surface assisted by pre-deposited Au film

H. Z. Yang¹ · G. D. Jiang¹ · W. J. Wang¹ · X. S. Mei¹ · A. F. Pan¹ · Z. Y. Zhai¹

Received: 15 April 2017 / Accepted: 30 August 2017 / Published online: 14 September 2017
© Springer-Verlag GmbH Germany 2017

Abstract With greater optical penetration depth and lower ablation threshold fluence, it is difficult to directly fabricate large scales of laser-induced periodic surface structures (LIPSSs) on indium–tin–oxide (ITO) films. This study proposed an approach to obtain optimized LIPSSs by sputtering an Au thin film on the ITO film surface. The concept behind the proposal is that the upper layer of the thin Au film can cause surface energy aggregation, inducing the initial ripple structures. The ripples deepened and become clear with lower energy due to optical trapping. The effective mechanism of Au film was analyzed and verified by a series of experiments. Linear sweep, parallel to the laser polarization direction, was performed using a Nd:VAN laser system with 10-ps Q-switched pulse, at a central wavelength of 532 nm, with a repetition rate of 1 kHz. The complete and clear features of the nanostructures, obtained with the periods of approximately 320 nm, were observed on ITO films with proper laser fluence and scanning speed. The depth of ripples was varying in the range of 15–65 nm with clear and coherent ITO films. The preferred efficiency of fabricating nanostructures and the excellent results were obtained at a scanning speed of 2.5 mm/s and a fluence of 0.189 J/cm². In this way, the ablation and shedding of ITO films was successfully avoided. Thus, the proposed technique can be considered to be a promising method for the laser machining of special nonmetal films.

1 Introduction

The formation of surface nanostructures on a wide variety of materials has great technological impact in application areas, such as catalysis, photonics, single electron and quantum devices, plasmonics, or solar cells [1, 2]. This potential has increased the number of research groups focusing on the generation and evolution of the nanostructures. Several investigations have been conducted on etching manufacturing (plasma drying etching) and additive manufacturing (CVD processes) to obtain the nanostructures on the surface of thin films [3, 4]. However, the required complex processes of the above-mentioned methods are the main issues that impede their promotion. Laser processing is not only simple and easy as a technological process, but also can produce fine nanostructures. The formation of laser-induced periodic surface structures (LIPSSs) has become of great interest at present [5, 6]. The LIPSSs can generally be obtained on semiconductors [7, 8], bulk metals [9, 10], and dielectrics [11] by ultrafast lasers. In particular, the interest in processing LIPSSs on thin films has increased due to the adjustment of film properties [12–14].

Indium–tin–oxide (ITO) films, a high carrier concentration semiconductor of low electrical resistivity and high transparency at visible light wavelengths, are widely used in transparent electrodes for display devices, transparent coating for solar energy heat mirrors, and window films in n–p heterojunction solar cells [15, 16]. Furthermore, as a wide band-gap semiconductor (3.5–4.3 eV), ITO films show high transmissibility in the visible and near-IR regions of the electromagnetic spectrum [17], which is significantly different from that of metal films. The generation and evolution of the nanostructures on ITO films surface is an important approach for adjusting the photoelectric characteristics (sheet resistance [18, 19] and surface reflection [20],

✉ W. J. Wang
wenjunwang@mail.xjtu.edu.cn

¹ State Key Laboratory for Manufacturing System Engineering, Xi'an Jiaotong University, Xi'an 710054, China

in particular). By tuning the structures of LIPSSs on thin transparent films, the spectral reflectance can affect the solar absorptance due to the nanostructures on the surface [21]. As a consequence, the research of LIPSSs on ITO films surface is extremely essential.

However, at present, most of the researchers are focusing on patterning ITO thin films [22–24]. A limited number of studies are focused on nanoscale periodic structures, which can be obtained by complex subsequent processing (i.e., chemical etching [6]), after laser irradiation, or solely obtaining incomplete nanostructures [25, 26], due to the special optical properties of ITO thin films. Unlike metal films [27, 28], it is difficult to directly fabricate coherent LIPSSs on nanoscale ITO films, owing to its long penetration depth and low damage threshold [19]. With the microscale of optical penetration depth, a large amount of photoelectrons are emitted on the bottom of the film, which lead to the static instability in the bottom of the film [29]. At this point, the energy absorption at the interface between ITO films and the substrate causes expansion and results in the ITO layer detached from the substrate and falls off partially. The resistivity of ITO films is significantly increased with surface shedding and also increased with the increased depth of nanostructures, which is difficult to control due to more energy deposition at the interface, significantly reducing the solar photovoltaic conversion efficiency. Therefore, it is better for obtaining the initial nanostructures when energy is limited on the surface of ITO film. The energy absorption on the formed initial structures due to optical trapping effect, and the depth of nanostructures can be controlled.

In this study, an approach of sputtering an Au thin film upon the ITO film as a protective and induced layer was proposed to obtain coherent and uniform LIPSSs with appropriate depth on transparent films. The optical absorption effect

of metal films can induce a large area of LIPSSs on ITO film surface owing to the laser that is focused on the surface of ITO film. With the relatively short penetration depth of 13 nm, Au was selected for this study due to its excellent physical characteristics and optical properties. To study the effects of sputtering Au films upon ITO films, the LIPSSs, directly obtained on ITO films under laser irradiation, were studied first. On this basis, the Au film was sprayed on ITO film and experiments were carried out at different laser fluences and scanning speeds. The depths of LIPSSs formed on ITO films are ranging, which significantly affect the photoelectric characteristics of the transparent films.

2 Materials and methods

In this study, a Nd:VAN picosecond laser system (High-Q, Austria) based on pulse regenerative amplification was used in the processing of ITO films. The laser system delivered pulses of 10 ps duration, with maximum power of 2 W, and 532 nm wavelength at a repetition rate of 1 kHz. The laser beam was focused on an almost circular spot of 45 μm diameter by a plano-convex lens (200 mm focal length) and is perpendicular to the samples surface. The energy density distribution of the laser beam was Gaussian with a beam quality factor (M^2) ~ 1.3 and the pulse energy was being adjusted using a combination of a half-wave plate and a linear polarizer.

ITO films with the thickness of 240 nm were deposited on glass substrates by magnetron sputtering (Denton Vacuum LLC Discovery 635). Then, the Au films with the thickness of 20 nm were coated onto ITO. Figure 1 shows the optical coefficient ratio $T/(1-R)$ and optical reflectivity (where T means transmissivity and R means reflectivity)

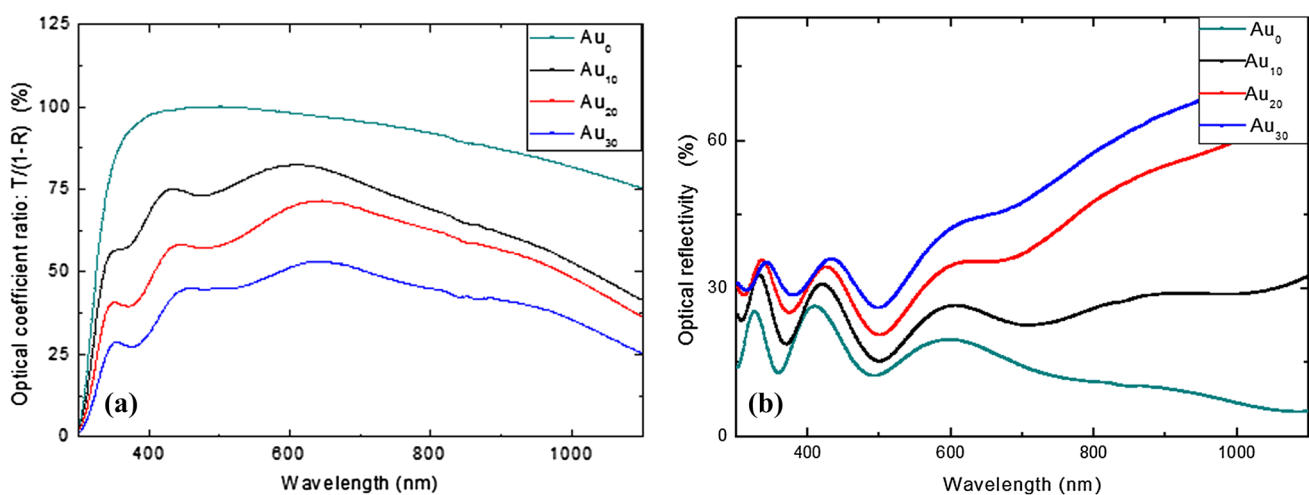


Fig. 1 Optical coefficient ratio: $T/(1 - R)$ and optical reflectivity at normal incidence of the Au sputtering samples in spectral range 300–1100 nm are shown in **a** and **b**, where T means transmissivity and R means reflectivity

of the ITO film coated with Au thin film of different thickness values, measured by UV–Vis–NIR (Shimadzu UV-3600) at a normal incidence within the spectral range 300–1100 nm. In addition, Au₁₀, Au₂₀, and Au₃₀ represent 10, 20, and 30 nm thickness of Au films, respectively, and Au₀ represents the ITO film without being coated with Au film. With the increase of Au layer thickness, it was clear that the reflectivity increased and transmissivity decreased, the energy absorption significantly increased on the upper layer of Au film. Therefore, the energy transferring at the bottom of ITO films was decreased and the integrity of ITO films can be guaranteed. Since the 20 nm film thickness with a proper absorption is slightly higher than the Au optical penetration depth of 13 nm, the negative effect of a nonuniform laser coupling field caused by direct excitation can be avoided [30].

The samples were fixed on a motorized xyz stage (OWIS, PS-30) for precise positioning. The samples were processed with a single scanning for each set of parameters. All the laser ablation experiments were performed in air. The schematic diagrams of the interaction of laser beam with the samples surface, when the beam arrives perpendicularly, are shown in Fig. 2a, b. The morphology of the LIPSSs of samples was observed using scanning electron microscopy (SEM, SU-8010), atomic force microscopy (AFM, INNOVA), and fast Fourier transform (FFT). An ultraviolet spectrometer (Shimadzu UV-3600) was used to measure the absorbance of the prepared films.

The texture structures of the ITO films were altered and characterized with various LIPSSs.

3 Results and discussion

3.1 Direct irradiation of ITO films by picosecond laser

Traditionally, the LIPSSs are obtained on bulk and film materials by the direct irradiation of an ultrafast laser. However, it is difficult to obtain coherent and uniform LIPSSs on ITO films with this method, due to its special photoelectric properties, as mentioned above. The experimental results by direct absorption of the laser beam at different fluences are shown in Fig. 3. The FFT profiles of LIPSSs with period perpendicular to laser polarization are demonstrated by the red-dotted square insets, respectively. Laser fluence of 0.43 J/cm² and a scan speed of 0.1 mm/s (the effective shots number is approximately 450 pulses) were applied to form LIPSSs, as shown in Fig. 3a. The fluence is slightly below the ablation threshold of ITO films in these experiments [19, 31]. Ripples were formed on ITO films and their spatial period turned out to be 435 nm. In addition, some ripples split and the period was 185 nm. The yellow-dotted square highlights a large area of ablation and shedding of ITO films in the center. It would greatly increase the surface resistance of ITO films. Even though a lower fluence of 0.31 J/cm² was applied, ablation and shedding of ITO films

Fig. 2 Schematic diagrams of picosecond laser irradiation acted on the samples: **a** laser is focused on the ITO film directly, **b** laser is focused on the Au thin film sputtering upon ITO film surface

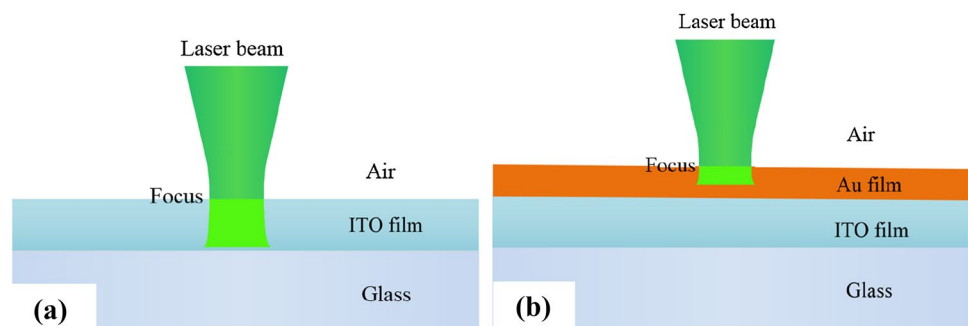
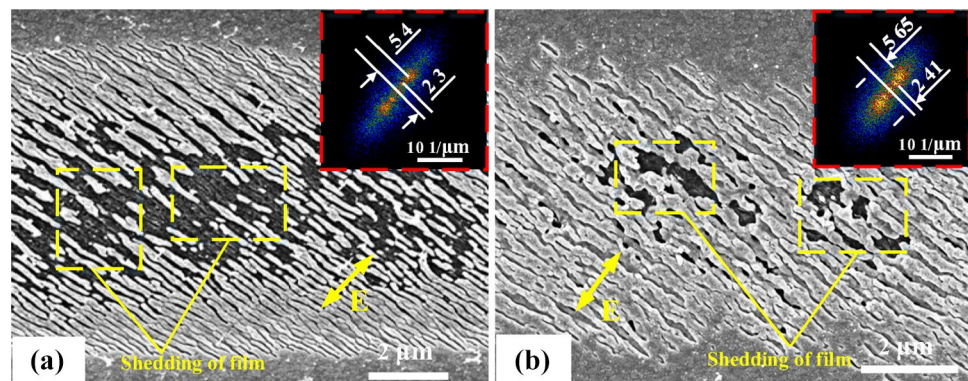


Fig. 3 SEM micrographs of nanostructures with laser beam focused on ITO film directly, at laser fluence of **a** 0.52 J/cm², and **b** 0.31 J/cm², scanning speed of 0.1 mm/s. The inset graphs show the FFT patterns and their cross-sectional profiles at locations corresponding to **a** and **b**. The arrow represents the direction of the laser polarization



also existed within the yellow-dotted squares, as shown in Fig. 3b. As previously mentioned, more energy absorption at the interface of substrate and ITO film with high transmittance lead to interface erosion. It is also obvious that the ripples are shallow and the laser fluence was not sufficient to produce any uniform surface texture at the edge of the laser-absorbed zone. The modified surface morphology of ITO films was caused by multiphoton absorption, resulting from photoionization and the formation of more free electrons, where the material absorbed more energy [32]. Therefore, the ITO film would also be processed below the ablation threshold as the laser fluence is enhanced; this leads to the ITO film being easily ablated and LIPSSs with clear and complete features are difficult to obtain. Nanostructures are inevitably destroyed only by direct laser irradiation of ITO films, which will significantly affect the structure morphology and properties.

3.2 Nanostructures formed on ITO film surface-assisted by pre-deposited Au film

To improve quality and obtain perfect nanostructures on ITO films, this paper proposes the use of Au thin film sputtering on ITO films surface. With short penetration of 13 nm, Au films of 20 nm will lead to energy aggregation in the upper layer, which will absorb the excessive heat. Before Au films are damaged and ablated, the laser energy is concentrated on the Au film and transferred to the ITO film surface, avoiding the ablation of the bottom of ITO film. In addition, with high thermal conductivity of Au films [33], the distribution of electron density becomes rapidly uniform on the Au films, thus avoiding the localized ablation and shedding of the ITO film.

Furthermore, when laser is focused on the upper layer of Au films, the original nanostructures are created in the Au film. Compared with transparent ITO film, the upper layer of Au films can capture more energy and obtain nanostructures with lower energy due to short penetration. With the effect of light trapping, the nanostructures will extend to the surface of ITO film layer with this lower energy, avoiding interface ablation between the ITO film and substrate. Accordingly, the uniform and clear ripples will be formed on the ITO film. Hence, the optimum LIPSSs will be obtained using Au films sputtered on ITO films surface. A series of experiments were carried out to illustrate the effect of the Au film on the fabrication of LIPSSs and explore the influence of laser energy and shots number on ITO film coated with a 20 nm thickness of Au layer, under the same conditions with those of the experiments of direct irradiation of ITO films.

Figure 4 shows the results obtained at a scanning speed of 0.6 mm/s, and the effective shots number is approximately 75. The Au film was ablated with a laser fluence of 0.044 J/cm² and the ITO film was remained intact, as shown

in Fig. 4a. Figure 4b1, c1 shows the high magnifications of the center and edge of the laser-absorbed zone, respectively. LIPSSs on Au films were obtained at the edge, which is shown in Fig. 4c1. Also some initial periodic structures were formed on ITO films surface in the center of the laser-absorbed zone, where the Au film was ablated, as shown in Fig. 4b1. The direction of the periodic structures was perpendicular to the polarization. The graphs of FFT are shown in Fig. 4b2, c2, respectively. The presence of the unclear initial periodic structures increased the roughness of ITO surface and contributed to obtaining distinct LIPSSs on ITO films surface. However, it was obvious that the Au film was not ablated completely and the unclear nanostructures cannot meet the requirements of the application with the low laser fluence. With the laser fluence increased to 0.142 J/cm², the width of ablated Au film increased. That is to say, Au films are removed both in the center and at the edge of the irradiation area, and ripples are obtained in the irradiation center on the ITO film surface, as shown in Fig. 4d. Figure 4e1, f1 shows the high magnifications in and out of the laser-absorbed edge, respectively. The corresponding elemental analysis chart is conducted to check whether gold is left on the surface after processing, as shown in Fig. 4e2, f2, respectively. Thus, it can be seen, despite the lower fluence at the edge in the ablation region, Au films are removed completely. High laser fluence was provided to obtain distinct LIPSSs on ITO films in the experiments of the present study.

3.3 Effect of laser fluence on the fabrication of nanostructures on ITO film

Figure 5 shows the LIPSSs fabricated on the surface of the sample with laser fluence in the range between 0.063 and 0.189 J/cm², at a scanning speed of 0.6 mm/s. The Au thin films were ablated completely in these processing conditions and the LIPSSs were more pronounced at higher laser fluence. The periods are signed at the peak of LIPSSs in (b2) and (c2), and the periods of ripples which are approximately 320 nm with the orientations are perpendicular to the laser polarization. It is clear that well-defined LIPSSs on complete ITO films surface existed in the laser-absorbed region and the morphology of LIPSSs are shallow at the laser fluence of 0.063 J/cm², as shown in Fig. 5a. The uniform and coherent LIPSSs can be formed at the laser fluence of 0.126 J/cm², and there is no damage of the ITO film, as shown in Fig. 5b. When the laser fluence continued increasing to 0.157 J/cm², more pronounced LIPSSs with sharper contrast can be obtained, but some ablation pits appeared on the ITO film to break in the uniform LIPSSs, as demonstrated in Fig. 5c. With clear and complete LIPSSs of Fig. 5b, c, the FFT is highlighted in the red-dotted square inset, respectively. Furthermore, the AFM measurements are shown in Fig. 5b1,

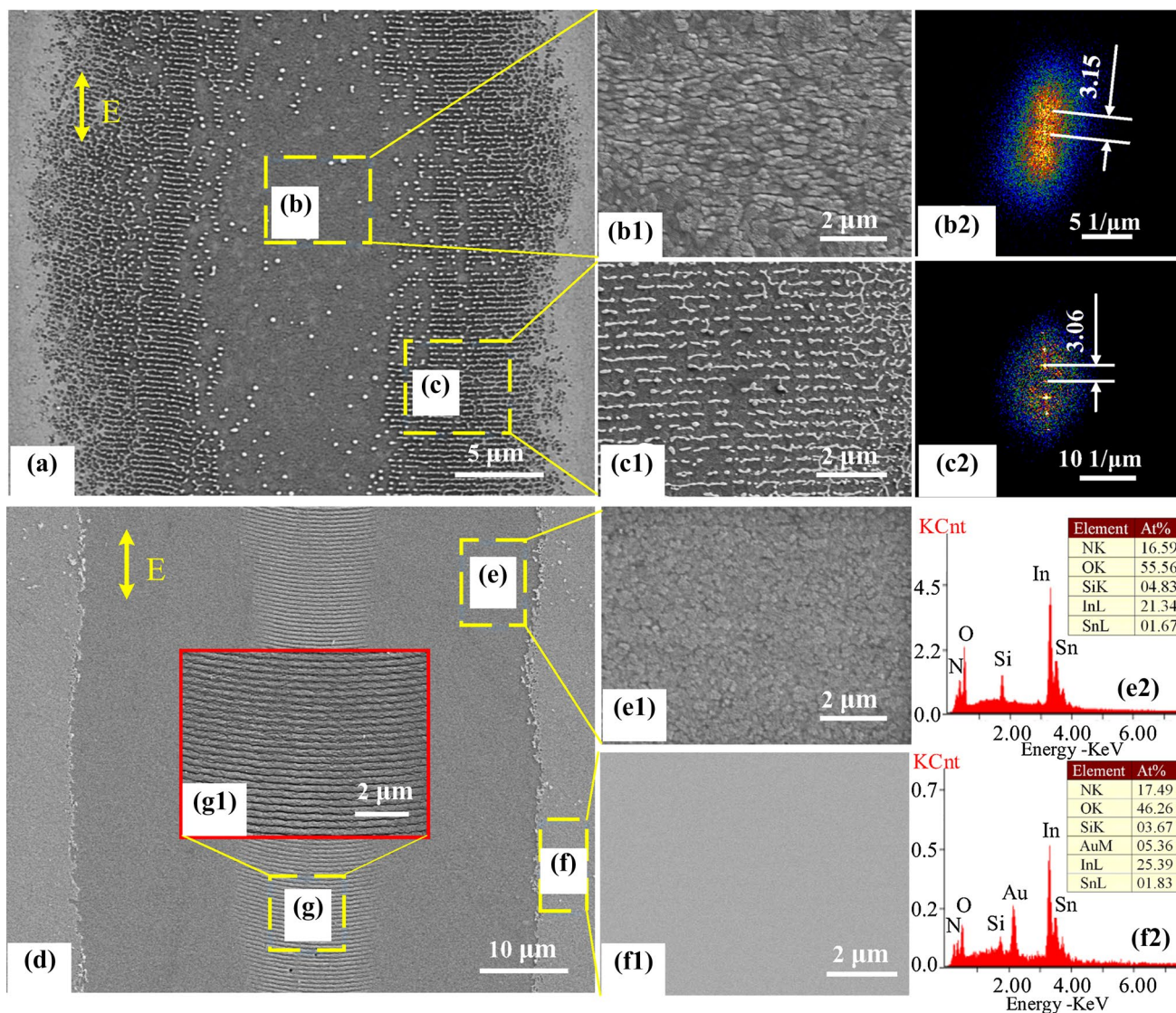


Fig. 4 SEM micrographs of nanostructures at scanning speed of 0.6 mm/s: **a** SEM micrograph of laser fluence of 0.044 J/cm², **b1** and **c1** are the high magnifications of the center and edge of laser-absorbed region accompanied by the FFT **b2** and **c2**, respectively. **d** SEM micrograph of laser fluence of 0.142 J/cm²; **e1** and **f1** are the

high magnifications in and out of laser-absorbed region accompanied by the elemental analysis **e2** and **f2**, respectively. **g1** is the high magnification of laser irradiated center **g**. The arrow represents the direction of the laser polarization, and the scanning direction parallel to the polarization direction

c1, and the corresponding topography profiles are shown in Fig. 5b2, c2. As can be seen, the depth of LIPSSs increased from 21 to 65 nm, more than 100 nm at the pits, and the periods are insignificantly altered with the increase of the laser fluence. Furthermore, definite grooves and ridges are formed on the sample surface with laser fluence of 0.189 J/cm², and glass substrate is exposed in some part of the laser-absorbed zone. That is, the Au thin film is ablated completely and part of the ITO film is also ablated, as shown in Fig. 5d. Thus, the coherent and distinct LIPSSs with proper depth can be obtained with the laser fluence of 0.126 J/cm², at a scanning speed of 0.6 mm/s, which can achieve the requirements well.

3.4 Effect of scanning speed on the fabrication of nanostructures on ITO film

Although the coherent LIPSS with a certain depth on complete ITO film can be formed with the fluence of 0.126 J/cm² at a scanning speed of 0.6 mm/s, higher power with higher processing speed were applied to improve efficiency. In this regard, the energy absorbed at the fixed position of the sample surface is considerable and the efficiency was substantially improved. As a result, the surface morphologies at different scan speeds in the condition of the fixed laser fluence of 0.189 J/cm² were discussed.

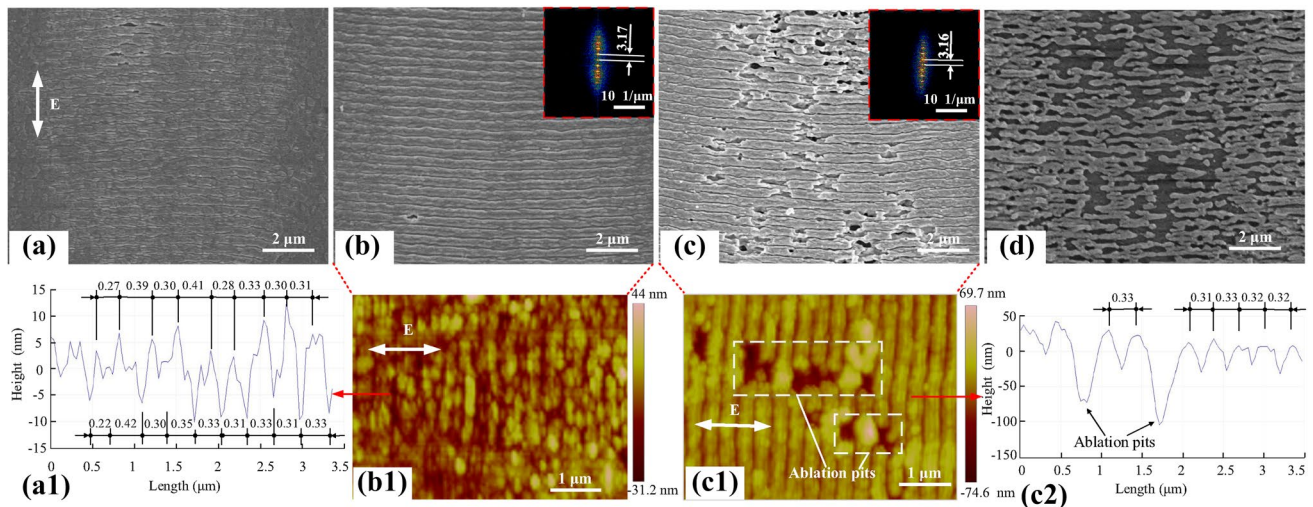


Fig. 5 SEM micrographs of nanostructures obtained on the ITO film induced by Au sputtering at a scanning speed of 0.6 mm/s and different fluence of **a** 0.063, **b** 0.126, **c** 0.157, and **d** 0.189 J/cm². The FFT of **b** and **c** is highlighted in the *red-dotted square inset*, respectively.

In addition, the AFM measurements and corresponding topography profiles are shown in **b1**, **b2**, and **c1**, **c2**, respectively. The periods are signed at the peak or valley of LIPSSs in **b2** and **c2**

The transformation of the nanostructures with the same absorbed fluence at different speeds is presented in Fig. 6. It can be concluded that the Au thin films were originally completely ablated and the LIPSSs had a high variation at the scanning speed, ranging from 0.5 to 5 mm/s. When the speed is less than 0.5 mm/s, most of the ITO films are ablated as more spots overlap and the cumulative energy exceeds the

ablation threshold in part of the irradiation region. For example, some of the LIPSSs were broken and fell off in the middle of the scanning area and the glass substrate was exposed, as shown in Fig. 6a. The periodic structures become coherent at the scanning speed of 1 mm/s, as shown in Fig. 6b. In addition, some pits exist in the intersection of the periodic ripples and the ripples are neither very uniform nor straight.

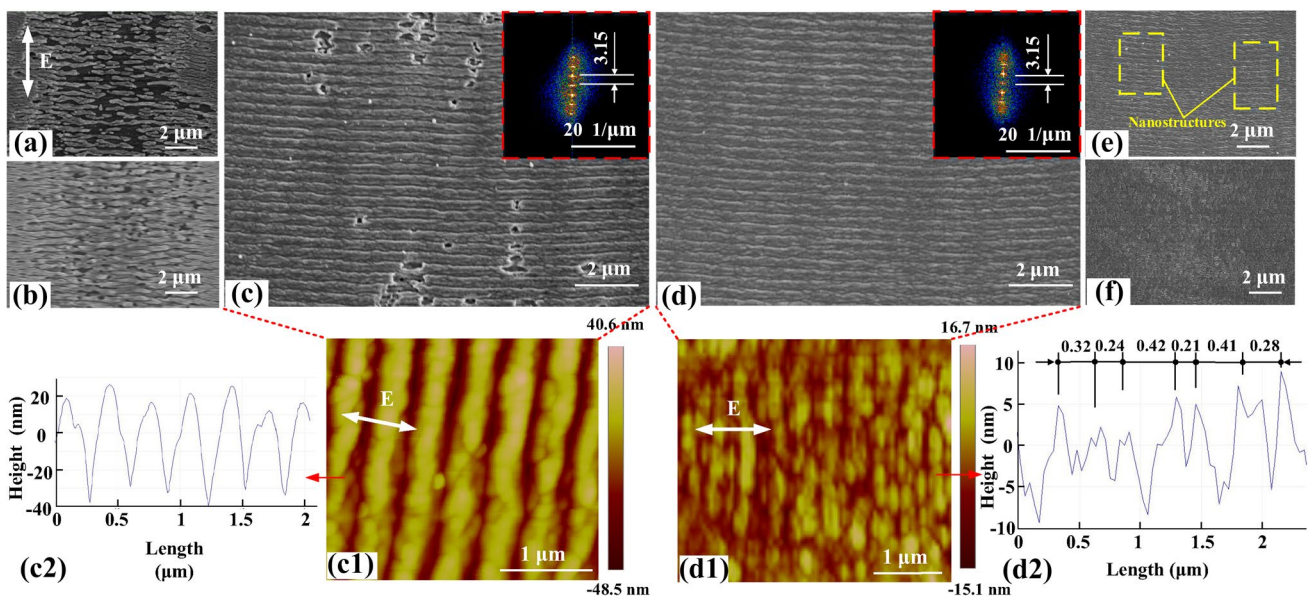


Fig. 6 SEM micrographs of nanostructures obtained on ITO films induced by Au sputtering with fluence of 0.189 J/cm² and different scanning speed: **a** 0.5 mm/s, **b** 1 mm/s, **c** 2 mm/s, **d** 3 mm/s, **e** 4 mm/s, and **f** 5 mm/s. The FFT graphs of **c** and **d** are highlighted

in the *red-dotted square insets*, respectively. In addition, the AFM measurements and corresponding topography profiles are shown in **c1**, **c2**, and **d1**, **d2**, respectively. The periods are signed at the peak of LIPSSs in **d2** for a better identification

Figure 6c shows the uniform and distinct periodic ripples that were formed at the speed of 2 mm/s. The depth is about 65 nm. Some individual pits could be observed on the ITO film surface, because some oxide particles were formed in the process. The ITO thin films with pits were not coherent and thus affected the electrical conductivity significantly. The uniform and coherent LIPSSs were fabricated on ITO films at the scanning speed of 3 mm/s, as shown in Fig. 6d. The depth is uneven in the range of 7–15 nm. The morphology is blurred and indistinct with the greater speed of 4 mm/s. The nanostructures only exist in partial region of laser irradiation area, as shown in the yellow-dotted squares of Fig. 6e. The features of the structures are difficult to distinguish at the speed of 5 mm/s, as shown in Fig. 6f. The graphs of FFT of Fig. 6c, d are presented in the red-dotted square insets, respectively. In addition, the AFM measurements and corresponding topography profiles are shown in Fig. 6c1, c2, d1, d2, respectively. The periods are signed at the peak of LIPSSs in (d2) for better identification. As can be seen, the change of ripples depth was decreased from 56 to 15 nm and the periods of ripples showed insignificant changes compared to the higher scanning speed. Thus, optimal structures can be obtained with the laser fluence of 0.189 J/cm^2 at a scanning speed of 3 mm/s, which can achieve the requirements well.

3.5 Systemic experiment and optimization result

In addition, a systemic experimental study was performed to investigate the effect of laser fluence ($0.032\text{--}0.252 \text{ J/cm}^2$) and the scanning speed ($0.05\text{--}5 \text{ mm/s}$, corresponding to the spot overlap number between 9 and 900) for the same conditions tested on the LIPSSs. Four distinctive regions were

identified, as shown in Fig. 7a. The detailed SEM images for the nanostructures in different regions show in Fig. 7b–e, respectively. The different regions correspond to the different nanostructures of the change of laser scanning speed and fluence that were discussed. With fluence values below 0.032 J/cm^2 , the surface films were intact and no structure was formed. Nanostructures were observed only on Au films with the laser fluence between 0.032 and 0.044 J/cm^2 , less than 800 spot overlap (region I). The Au films were ablated completely and some shallow morphology of structures was observed on ITO films with fluence between 0.044 and 0.063 J/cm^2 and spot overlap numbers between 1 and 1000 (region II). A large area of nano-ripples could be observed with a fluence between 0.063 and 0.252 J/cm^2 , and corresponded to spot overlap numbers less than 880 (region III). With higher fluence or spot overlap numbers, the ITO films were also ablated in the center of the irradiated laser beam and the glass substrate was exposed (region IV). The periods were essentially unchanged with different fluence and slightly fluctuate at higher scanning speed in the range of this experiment.

Although large area of structures can be obtained in region III of Fig. 7, various kinds of defects (for instance, ablation pits or unclear nanostructures) still existed in some experiments. The satisfactory results can be obtained at a scanning speed of 2.5 mm/s and a fluence of 0.189 J/cm^2 , as shown in Fig. 8a. The graphs of FFT are highlighted in the red-dotted square inset. The AFM measurement and corresponding topography profile are shown in Fig. 8b, c, respectively. The period was 320 nm , which is approximately equal to the period obtained on Au film with low laser fluence, as shown in Fig. 4. It is widely accepted that the Au film can assist surface plasmon laser coupling to dominate the

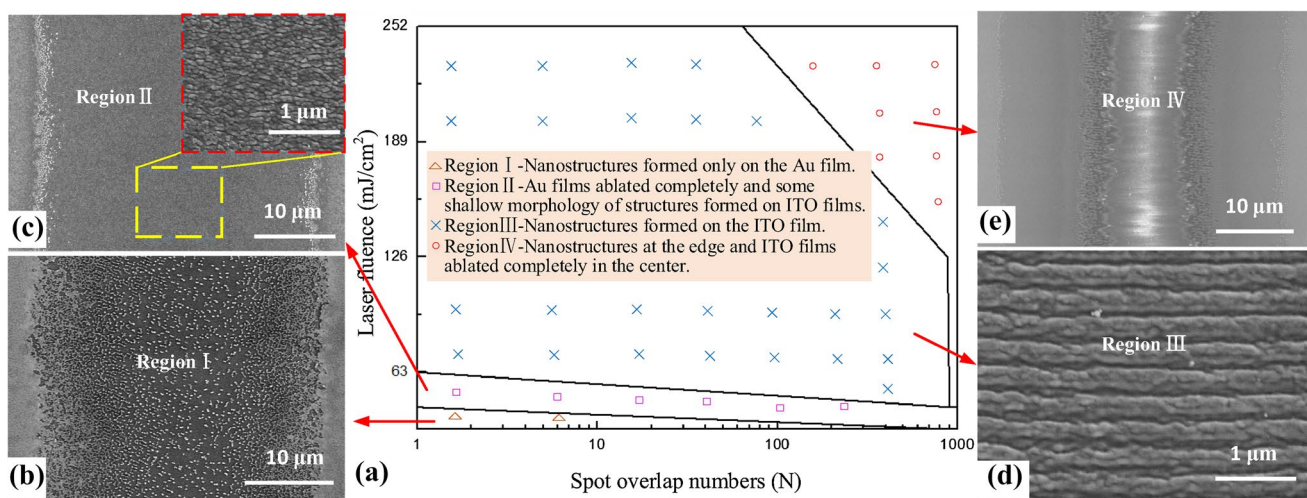
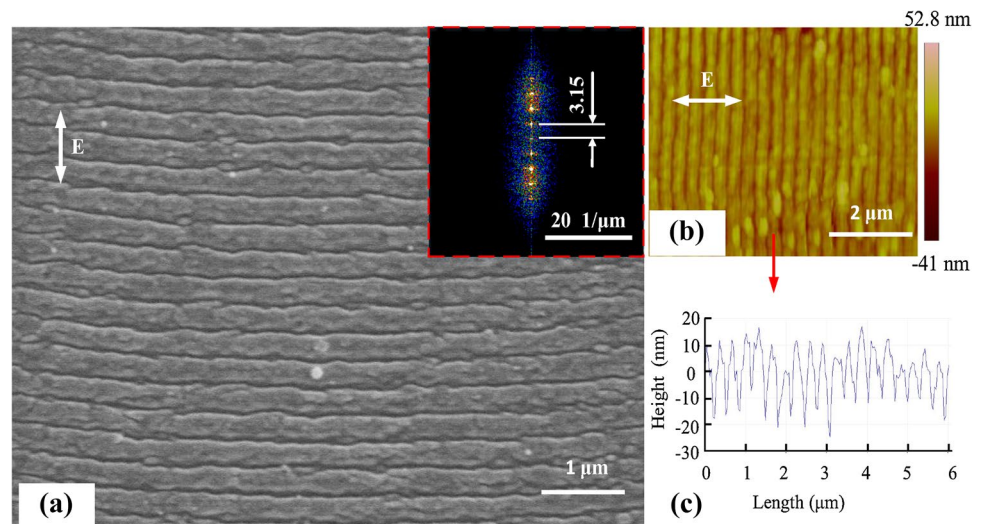


Fig. 7 a Summary of selected spot overlap numbers (9–900) and laser fluence ($0.032\text{--}0.252 \text{ J/cm}^2$) conditions, where different nanostructures were induced by 20 nm Au film sputtering on 240 nm ITO

surface at a wavelength of 532 nm. b–e Detailed SEM images for the nanostructures in different regions I–IV, respectively

Fig. 8 **a** SEM micrograph of nanostructures on the ITO film induced by Au sputtering at a scanning speed of 2.5 mm/s and fluence of 0.189 J/cm². The FFT profiles are highlighted in the red-dotted square inset. **b**, **c** AFM measurement and corresponding topography profile, respectively



evolution of LIPSSs by the interference between the incident laser and surface plasmon [34, 35]. The depth of LIPSSs on ITO films surface is approximately 40 nm, which can be observed by the cross-section profile. The proper depth of LIPSSs can prevent the defects of ITO films and ensure good electrical conductivity. Thus, preferable efficiency and excellent results can be achieved by selecting the proper parameters.

From the results above, it can be concluded that Au films are a great assistance of processing periodic nanostructures on ITO film surface. Based on Au sputtering, not only the coherent LIPSSs were achieved, but also the depth of LIPSSs was controlled in the range 15–5 nm, without any damage. With the decrease of optical coefficient ratio after sputtering Au film (Fig. 1), most of the light wave was absorbed and reflected by the high density of electrons. The energy of the incident light to ITO films was gradually decreased, and the uniform and coherent nanostructures were formed on transparent conductive ITO films. As the inducing layer, Au films could successfully improve the effect of processing LIPSSs in this study.

4 Conclusions

This study proposed an approach for obtaining perfect LIPSSs induced by Au thin film sputtering on ITO film surface. The mechanism of action of Au film was analyzed and verified by a series of experiments. The upper layer of Au film can aggregate the surface energy and protect the lower layer of ITO film. With the fluence in a certain range from 0.063 to 0.189 J/cm² at the scanning speed of 0.6 mm/s, and the scanning speed in the range of 0.5–4 mm/s at the fluence of 0.189 J/cm², the regular ripples can be obtained. The periods of LIPSSs on ITO films were approximately 320 nm

and almost constant with the different fluence and scanning speed values. The depth of clear ripples was varying in the range 15–65 nm on ITO films. The complete and satisfactory nanostructures without any damage were obtained on ITO films induced by Au films with the fluence of 0.189 J/cm², at a scanning speed of 2.5 mm/s. The depth is about 40 nm. The nanostructures with controllable periods and depths on the surface can adjust the photoelectric characteristics of semiconductor films, which help the industrial application of this technology. In addition, the proposed technique can be considered to be a promising method for the laser machining of special nonmetal films.

5 Acknowledgements

This work was supported by the National Key Research and Development Program of China (Grant no. 2016YFB1102502), the National Natural Science Foundation of China (Grant nos. 51475361, 91323303, and 51421004), and the Program for Changjiang Scholars and Innovative Research Team in University (Grant no. IRT_15R54).

References

1. D.L. Feldheim, C. Foss, *Behav. Brain Res.* **14**, 183–207 (2002)
2. P. Moriarty, *Rep. Prog. Phys.* **64**, 297–381 (2001)
3. C. Xu, L. Deng, A. Holder, L.R. Bailey, C. Leendertz, J. Bergmann, G. Proudfoot, O. Thomas, R. Gunn, M. Cooke, *Phys. Status Solidi A* **212**, 171–176 (2014)
4. A. Khosroabadi, P. Gangopadhyay, B. Duong, J. Thomas, A.K. Sigdel, J.J. Berry, T. Gennett, N. Peyghambarian, R.A. Norwood, *Phys. Status Solidi* **210**, 831–838 (2013)
5. J. Young, J. Preston, H. Van Driel, J. Sipe, *Phys. Rev. B* **27**, 1141–1154 (1983)

6. C.W. Chenga, I.M. Leeb, J.S. Chen, *Appl. Surf. Sci.* **316**, 9–14 (2014)
7. J. Bonse, A. Rosenfeld, J. Kruger, *J. Appl. Phys.* **106**, 104910 (2009)
8. F. Costache, S. Kouteva-Arguirova, J. Reif, *Appl. Phys. A* **79**, 1429–1432 (2004)
9. S. Sakabe, M. Hashida, S. Tokita, S. Namba, K. Okamuro, *Phys. Rev. B* **79**, 033409 (2009)
10. J. Bonse, J. Krüger, S. Höhm, A. Rosenfeld, *J. Laser Appl.* **24**, 0420006–0420012 (2012)
11. A. Rosenfeld, M. Rohloff, S. Höhm, J. Krüger, J. Bonse, *J. Appl. Phys.* **110**, 014910 (2011)
12. K. Taweessup, I. Yamamoto, T. Chikyow, G. Lothongkum, K. Tsukagoshi, T. Ohishi, S. Tungasmita, P. Visuttipitukul, K. Ito, K. Tsukagoshi, T. Ohishi, S. Tungasmita, P. Visuttipitukul, K. Ito, M. Takahashi, T. Nabatame, *Thin Solid Films*. **598**, 126–130 (2016)
13. T.-L. Chang, Z.-C. Chen, Y.-C. Lee, *Opt. Express* **20**, 168372 (2016)
14. R. Saha, W.D. Nix, *Acta Mater.* **50**, 23–38 (2002)
15. H. Kim, C.M. Gilmore, A. Piqué, J.S. Horwitz, H. Mattoussi, H. Murata, Z.H. Kafafi, D.B. Chrisey, *J. Appl. Phys.* **88**, 6021–6025 (2000)
16. J.O. Park, J.H. Lee, J.J. Kim, S.H. Cho, Y.K. Cho, *Thin Solid Films* **474**, 127–132 (2005)
17. F. Ruffino, E. Carria, S. Kimiagar, I. Crupi, F. Simone, M.G. Grimaldi, *Sci. Adv. Mater.* **4**, 708–718 (2012)
18. N. Tagawa, M. Takada, A. Mori, H. Sawada, K. Kawahara, *Tribol. Lett.* **24**, 143–149 (2006)
19. J. Eichstädt, G.R.B.E. Römer, A.J. Huis int Veld, *Phys. Proc.* **12**, 7–15 (2011)
20. A.Y. Vorobyev, V.S. Makin, C. Guo, *Phys. Rev. Lett.* **102**, 269401 (2009)
21. L. Kotsedi, Z.Y. Nuru, P. Mthunzi, T.F.G. Muller, S.M. Eaton, B. Julies, E. Manikandan, R. Ramponi, M. Maaza, *Appl. Surf. Sci.* **321**, 560–565 (2014)
22. C. McDonnell, D. Milne, C. Prieto, H. Chan, D. Rostohar, G.M. O'Connor, *Appl. Surf. Sci.* **359**, 567–575 (2015)
23. S. Krause, P.T. Miclea, F. Steudel, S. Schweizer, G. Seifert, *EPJ Photovolt.* **4**, 40601 (2013)
24. H. Shin, B. Sim, M. Lee, *Opt. Laser Eng.* **48**, 816–820 (2010)
25. A. Rodríguez, M.C. Morant-Minana, A. Dias-Ponte, M. Martínez-Calderón, M. Gómez-Aranzadi, S.M. Olaizola, *Surf. Sci.* **351**, 135–139 (2015)
26. M. Straub, M. Afshar, D. Feili, H. Seidel, K. König, *Phys. Proc.* **12**, 16–23 (2011)
27. A. Ruiz de la Cruz, R. Lahoz, J. Siegel, G.F. de la Fuente, J. Solis, *Opt. Lett.* **39**, 2491–2494 (2014)
28. K. Zhang, J. Deng, Y. Xing, Y. Lian, G. Zhang, *Surf. Eng.* **31**, 271–281 (2015)
29. Q. Chen, M. Zhou, Z.M. Huang, *J. Funct. Mater.* **42**, 158–160 (2011)
30. P. Feng, L. Jiang, X. Li, W. Rong, K. Zhang, Q. Cao, *Appl. Opt.* **54**, 1314–1319 (2015)
31. S.Z. Xiao, E.L. Gurevich, A. Ostendorf, *Appl. Phys. A* **107**, 333–338 (2012)
32. P.S. Banks, B.C. Stuart, M.A. Komashko, M.D. Feit, A.M. Rubenchik, M.D. Perry, *Proc. SPIE* **3934**, 14–21 (2000)
33. J.B. Lee, S.H. Lee, *Mater. Trans.* **52**, 1492–1499 (2011)
34. M. Huang, F.L. Zhao, Y. Cheng, N.S. Xu, Z.Z. Xu, *ACS Nano* **3**, 4062–4070 (2009)
35. T.T.D. Huynh, A. Petit, N. Semmar, *Appl. Surf. Sci.* **302**, 109–113 (2014)